

Enforcing Reciprocity in Operator Learning for Seismic Wave Propagation

Caifeng Zou^{*1}, Yaozhong Shi², Zachary E. Ross¹, Robert W. Clayton¹, and Kamyar Azizzadenesheli³

¹Seismological Laboratory, California Institute of Technology, Pasadena, California, U.S.A.

²Division of Engineering and Applied Sciences, California Institute of Technology, Pasadena, California, U.S.A.

³Nvidia Corporation, Santa Clara, California, U.S.A.

Abstract

Accurate and efficient wavefield modeling underpins seismic structure and source studies. Traditional methods comply with physical laws but are computationally intensive. Data-driven methods, while opening new avenues for advancement, have yet to incorporate strict physical consistency. The principle of reciprocity is one of the most fundamental physical laws in wave propagation. We introduce the Reciprocity-Enforced Neural Operator (RENO), a transformer-based architecture for modeling seismic wave propagation that hard-codes the reciprocity principle. The model leverages the cross-attention mechanism and commutative operations to guarantee invariance under swapping source and receiver positions. Beyond improved physical consistency, the proposed architecture supports simultaneous realizations for multiple sources without crosstalk issues. This yields an order-of-magnitude inference speedup at a similar memory footprint over an reciprocity-unenforced neural operator on a realistic configuration. We demonstrate the functionality using the reciprocity relation for particle velocity fields under single forces. This architecture is also applicable to pressure fields under dilatational sources and travel-time fields governed by the eikonal equation, paving the way for encoding more complex reciprocity relations.

1 Introduction

Accurate and efficient modeling of seismic wave propagation is essential for subsurface structure imaging, ground motion simulation, and earthquake source inversion. Traditional numerical solvers, such as finite difference and finite element methods, have theoretical guidance for modeling accuracy and stability (e.g., the number of grid points required per wavelength). However, computational cost is often the primary bottleneck, particularly for large-scale inverse problems or applications requiring extensive parameter sweeps. The emergence of machine learning has offered promising pathways for accelerating seismic wavefield modeling.

Machine learning methods for solving partial differential equations (PDEs) are currently dominated by two lines of work: Physics-Informed Neural Networks (PINNs) (Raissi et al., 2019) and Neural

^{*}Corresponding author: czou@caltech.edu

Operators (Li et al., 2020b). The former approximates the solution function, while the latter learns the solution operator. Training a PINN is challenging, because it uses the PDE as a soft constraint, resulting in a highly non-convex loss landscape. Moreover, it only approximates the solution function to a single instance of the PDE family and requires retraining for different PDE parameters. Consequently, PINN applications in seismology are often constrained to a specific velocity model (Alkhalifah et al., 2021; Huang & Alkhalifah, 2022a,b; Rasht-Behesht et al., 2022; Ren et al., 2024; Song et al., 2021, 2022). Neural operators do not have these limitations, because they learn maps between function spaces from data (which could include simulations). They exhibit excellent generalization performance in modeling seismic wave propagation (Huang & Alkhalifah, 2025; Kong et al., 2025; Lehmann et al., 2024, 2025; Yang et al., 2021, 2023; Zou et al., 2024, 2025). However, neural operators are primarily data-driven (despite physics-informed variants (Li et al., 2024)) and often lack the precision of traditional solvers. Furthermore, they may violate physical laws if not explicitly constrained.

The reciprocity principle is a fundamental physical law in wave propagation that relates two seismic wavefields in a medium under interchange of source and receiver positions (Arntsen & Carcione, 2000; Knopoff & Gangi, 1959). This principle is most commonly used for efficient wavefield simulations where sources significantly outnumber receivers (Eisner & Clayton, 2001; Graves & Clayton, 1992), thereby facilitating source and structure inversion (Petrov & Newman, 2019; Zhao et al., 2006). Although its concise formula and ease of implementation cast reciprocity as an ideal constraint for training neural surrogates, this is sparsely documented. Only recently have Geng et al. (2025) and Wang et al. (2026) employed reciprocity as a soft constraint in training PINNs for travel-time simulation. However, hard-coding this physical symmetry into model architectures remains unexplored.

Here, we introduce the Reciprocity-Enforced Neural Operator (RENO), a transformer-based architecture that hard-codes the reciprocity principle into seismic wavefield modeling. RENO adheres to the physical law by explicit design, regardless of training, via the cross-attention mechanism and commutative operations. It enables simultaneous multi-source modeling, delivering an order-of-magnitude inference speedup over a standard neural operator on a real-world configuration. The proposed architecture directly applies to reciprocity relations for particle velocity fields under single forces, pressure fields under dilatational sources, and travel-time fields.

2 Preliminaries

2.1 Reciprocity relations

The reciprocity principle describes a certain invariance in a medium where the source and receiver positions are interchanged. The reciprocity relations are categorized by types of sources (e.g., single forces and force couples) and physical properties recorded at receivers (e.g., particle velocity, strain, and stress) (Arntsen & Carcione, 2000). In this study, we take the example of single forces and particle velocity fields, the reciprocity relation for which holds in inhomogeneous, anisotropic, viscoelastic media is

$$v_p^m(\mathbf{x}'_0, t; \mathbf{x}_0) = v_m^p(\mathbf{x}_0, t; \mathbf{x}'_0), \quad (1)$$

where $v_p^m(\mathbf{x}'_0, t; \mathbf{x}_0)$ indicates the p component of the particle velocity at position \mathbf{x}'_0 due to a body force acting in the m direction at position \mathbf{x}_0 as a function of time t . In the frequency domain, the

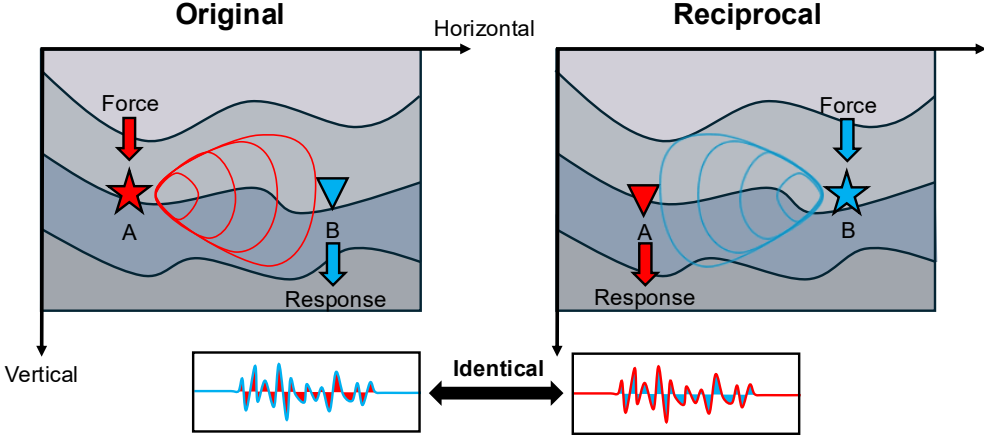


Figure 1: Schematic of the reciprocity relation for single vertical forces at sources and vertical particle velocity responses at receivers.

relation becomes

$$V_p^m(\mathbf{x}'_0, \omega; \mathbf{x}_0) = V_m^p(\mathbf{x}_0, \omega; \mathbf{x}'_0), \quad (2)$$

where V is the Fourier transform of v and ω is the angular frequency. To further simplify the problem, we only consider $m = p$ so that the directional force can be fixed. We focus on single vertical forces and vertical velocity fields, as the horizontal cases should be no different. Thus, the target variable is an invariant scalar when swapping the source and receiver. Figure 1 is a schematic for the reciprocity relation studied here. Future studies involving vectors or different types of sources and responses will be extensions of this pilot study.

2.2 Neural operators

Neural Operators are models for learning maps between function spaces, making them a rapid, powerful tool for solving PDEs (Azizzadenesheli et al., 2024; Li et al., 2020b). What distinguishes neural operators from classical neural networks is their discretization agnosticism: a model is not tied to a specific discretization or geometry. While Physics-Informed Neural Networks (PINNs) (Raissi et al., 2019) are also discretization-agnostic, they approximate the solution function for a specific instance. In contrast, neural operators are trained to learn a family of PDEs with varying parameters. Since their inception, this class of machine learning models has seen many variants. For example, the Fourier Neural Operator (FNO) speeds up computations via spectral-domain convolutions (Li et al., 2020a). The Geometry-Informed Neural Operator (GINO) integrates the ability of graph neural operators (GNOs) to handle irregular grids with the computational efficiency of FNOs (Li et al., 2023). The Physics-Informed Neural Operator (PINO) incorporates the function optimization capacity of PINNs into operator learning, combining advantages of both worlds (Li et al., 2024). More recent variants integrate transformers (Vaswani et al., 2017), which have demonstrated transformative success across various fields, to boost the performance and scalability of neural operators (Alkin et al., 2024; Shi et al., 2025; Wu et al., 2024).

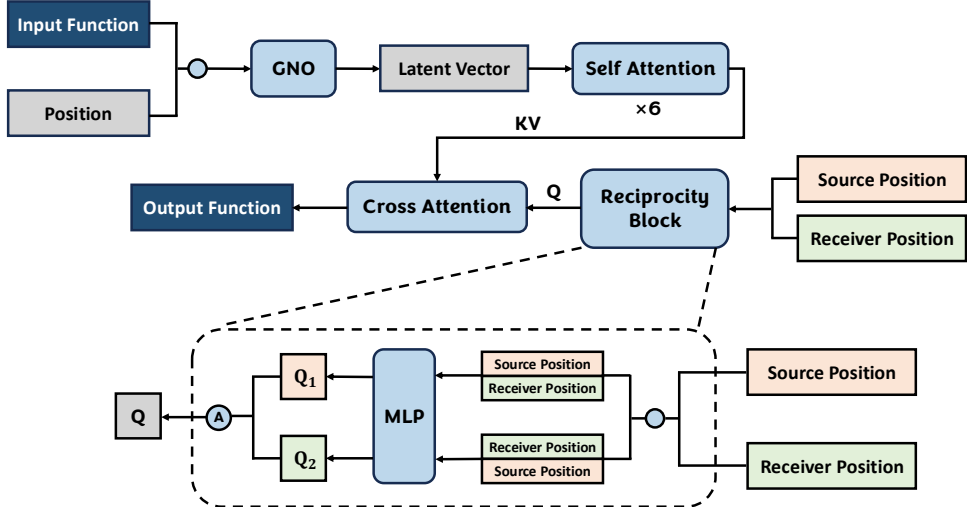


Figure 2: RENO architecture. Blue circles denote concatenation. A in the blue circle denotes an averaging operation. Q represents queries and KV represents key-value pairs. All positions are encoded using sinusoidal embeddings.

3 Methods

In this study, we develop a neural operator architecture that explicitly enforces reciprocity, referred to as RENO (Reciprocity-Enforced Neural Operator). Inspired by the Mesh-Informed Neural Operator (MINO) for generative modeling (Shi et al., 2025), we adapt its architecture to ensure reciprocal symmetry. Figure 2 outlines the RENO architecture. The input function is represented as a point cloud of values at discrete positions. Because the number of points is typically too large to be directly handled by transformers, a GNO is used to compress the input into a latent function represented by a small number of “super nodes”. This function can then be efficiently processed by self-attention layers. The GNO acts as a discretization-agnostic encoder, ensuring the architecture generalizes to arbitrary input geometries.

We highlight the Reciprocity Block, where reciprocity is made a hard constraint via a series of commutative operations. Specifically, the source and receiver positions are concatenated in both permutations and passed through the same Multi-Layer Perceptron (MLP). The resulting output vectors, Q_1 and Q_2 , are averaged to produce the final query. This query is then input to the cross-attention decoder to obtain solutions for the corresponding source-receiver pairs. Regarding concepts such as Q (query), KV (key-value), self- and cross- attention or more technical details, we refer the interested readers to Vaswani et al. (2017) and Shi et al. (2025).

To avoid complexity arising from the time dimension, we train a Helmholtz neural operator for frequency-domain solutions (Zou et al., 2024), so that both the input and output functions are two-dimensional in space. The input includes V_P , V_S , and the frequency value parameterized by a constant function. The output is the frequency-domain particle velocity solution for the queried source-receiver pair. The time-domain solution can be obtained via inverse Fourier transform.

4 Experiments

In this section, we compare the RENO with a baseline model that is not explicitly informed of reciprocity during training; rather this baseline model learns reciprocity implicitly by learning to solve the PDE. We remove the source-receiver symmetry in the model architecture and make the source location as an input feature along with velocity and frequency information (Zou et al., 2024, 2025). We query the waveform solutions at every grid point on the free surface for both models. We use synthetic data generated with a staggered grid finite difference solver (Richardson, 2025) to train the neural operators. The solver solves the isotropic elastic wave equation in the particle velocity-stress formulation. The elastic medium is parameterized by V_P , V_S , and density, of which V_S is generated from Matérn random fields sampled around a 1D model, and V_P and density are derived from it using empirical relations (Brocher, 2005). Each simulation has a single source, the location of which is uniformly sampled from the free surface. The source is a vertical force and the source time function is a Ricker wavelet with a central frequency of 0.3 Hz. The simulated wavefield lasts 50 s using a time step of 0.001 s, which is Fourier-transformed and filtered to [0.1, 0.5] Hz for use with the Helmholtz neural operator. The computational domain is 85 km (horizontal) \times 20 km (vertical) with 125 m spacing. For training, the medium parameters are downsampled by a factor of 2 for computational efficiency, resulting in a 339×81 grid. The neural operator is trained to solve for the vertical particle velocity field, for which the reciprocity relation holds under vertical forces.

4.1 Reciprocal generalization

We start with demonstrating the fundamental difference in how the reciprocity-enforced and unenforced models internalize physical laws. For the purpose of this basic demonstration, we fit both models to just a single simulation and evaluate them on the reciprocal solutions, where the source becomes the receiver and the receivers become sources. Figure 3 shows the results. Based on the reciprocity principle, the original and reciprocal solutions should be identical, as verified by the finite difference simulations in the first row. The RENO, trained to accurately fit the original simulation, generalizes to the reciprocal case with identical accuracy without prior exposure to such data, owing to the imposed hard-coded constraint. However, the standard operator without this constraint fails to generate any meaningful seismic signal in the reciprocal test, because it has not learned sufficient physics from a single simulation to generalize. This example suggests that, by enforcing reciprocity as an architectural constraint, the model can leverage physical symmetry to map unseen reciprocal pairs, effectively doubling the information underlying each training instance.

4.2 Learning behavior

Here, we study how the two models learn the physics when trained on a reasonable amount of data. We use a normalized ℓ_2 -norm as the loss function. A total of 10000 simulations are used for training and 1000 simulations are used for validation. We define the reciprocal error as

$$\text{Reciprocal error} = \frac{\|\mathcal{L}(\mathbf{x}_s, \mathbf{x}_r, *) - \mathcal{L}(\mathbf{x}_r, \mathbf{x}_s, *)\|_2}{\|\mathcal{L}(\mathbf{x}_s, \mathbf{x}_r, *)\|_2}, \quad (3)$$

where \mathcal{L} denotes the learned neural operator, \mathbf{x}_s and \mathbf{x}_r denote the source and receiver positions, respectively, and $*$ represents other input to the operator. Ideally, this error should be zero. For computational efficiency, a random source-receiver pair is selected from the validation set at each

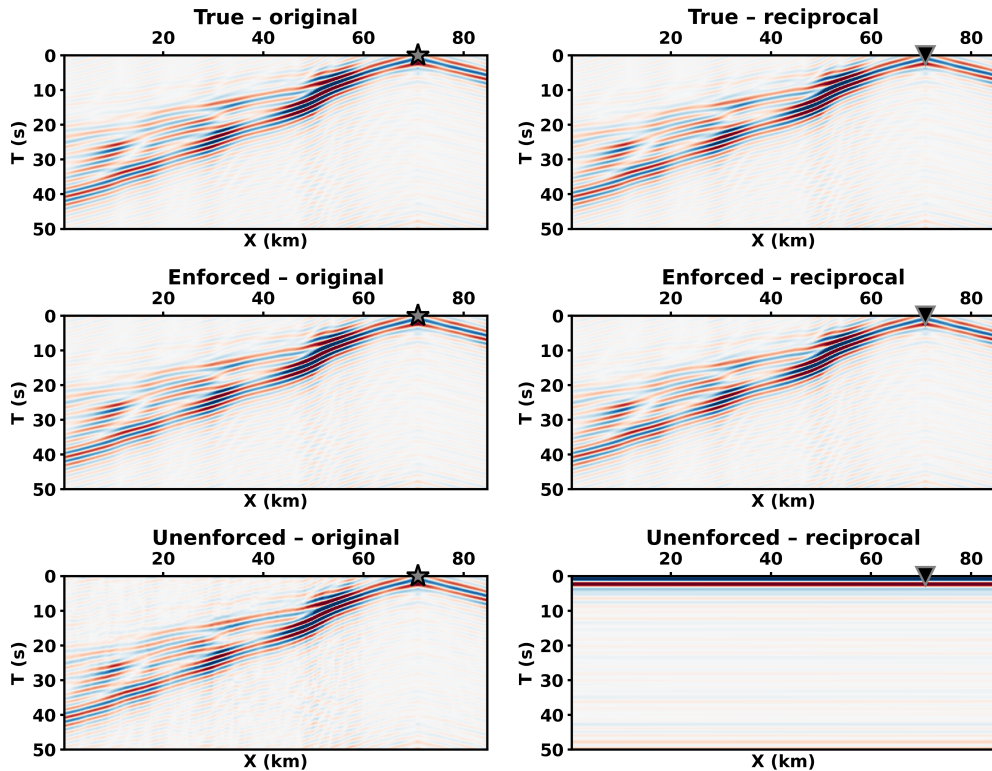


Figure 3: Reciprocal experiments where sources and receivers are swapped. The star marks the source, which becomes the receiver marked with a triangle in the reciprocal experiment. The first row shows the waveform solutions from the finite difference solver, taken as ground truth. The second and third rows show the predictions from the reciprocity-enforced and unenforced neural operators, respectively. Both models are trained on a single simulation shown on the left.

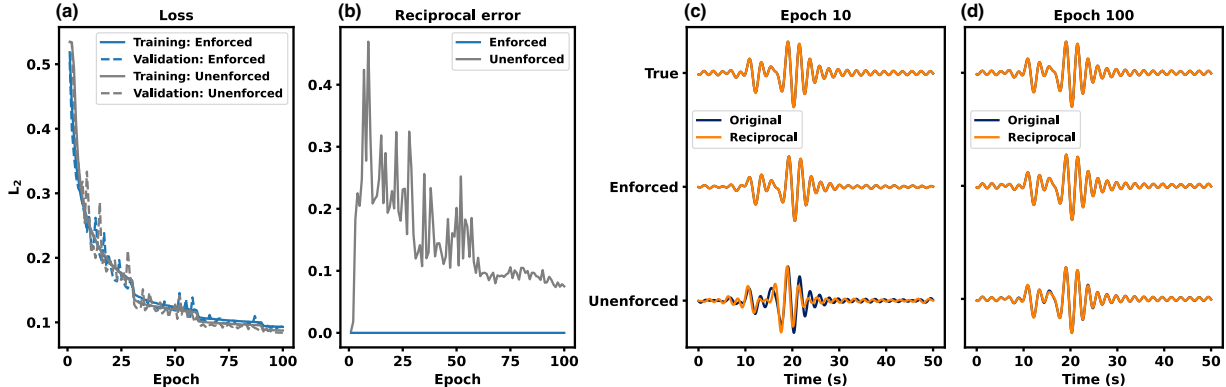


Figure 4: (a) Loss and (b) reciprocal error during training for the reciprocity-enforced and unenforced models. Validation examples of reciprocal waveforms at (c) epoch 10 and (d) epoch 100.

iteration to compute the reciprocal error. Figure 4a plots the ℓ_2 loss during training for the reciprocity-enforced and unenforced models, shown in blue and gray, respectively. This metric is computed over solutions at all receivers for a single source and thus does not honor the reciprocity principle but reflects averaged overall performance. In terms of the ℓ_2 loss, both models show similar accuracy ultimately, while the RENO performs better at earlier epochs. However, since reciprocity is not hard-coded in the baseline model, it can only acquire this property indirectly from data that obeys the physics of wave propagation. Although the model might ideally conform to the law by the end of training, this is not guaranteed in practice. As shown in Figure 4b, the reciprocal error of the baseline model generally decreases during training but does not ultimately reach zero. It is only zero at the beginning due to initialization. The RENO maintains zero reciprocal error, as designed. Figure 4c shows an example pair of reciprocal waveforms (the source and receiver positions of which are swapped) from validation data at an earlier stage of training. The RENO predicts both solutions accurately, whereas the baseline model is less accurate for both. Although the baseline model yields more accurate predictions as training progresses, it still fails to strictly adhere to reciprocity (Figure 4d). In summary, the RENO has the physical law hard-coded into its architecture, whereas a standard model must learn it from scratch. Although both models achieve comparable overall accuracy given proper training, the physics-embedded model converges faster and is expected to be more robust to changes in the experimental setup. Above all, it is a perfect model in terms of the reciprocity metric.

4.3 Computational efficiency

The source-receiver symmetry in the RENO architecture not only guarantees adherence to this physical principle but also enables computing solutions for multiple sources in a single query. Unlike standard operators or numerical solvers restricted to single-source formulations, this parallelization occurs within the query mechanism of the transformer backbone rather than at the batch level, thus significantly improving computational efficiency. Because there is no correlation between queried source-receiver pairs, arbitrarily many sources can be solved for simultaneously without crosstalk issues, provided there is sufficient memory.

Table 1: Computational efficiency and GPU memory usage for the reciprocity-enforced and unenforced models during inference. The comparison is made on a community velocity model with 234 sources and 339 receivers on the free surface, using an NVIDIA RTX A6000 GPU.

Model	Runtime (forward)	GPU Usage (forward)	Runtime (inverse)	GPU Usage (inverse)
Reciprocity-Enforced	0.31 s	18182 MB	27.25 s	2083 MB
Unenforced	9.34 s	18966 MB	750.96 s	2089 MB

We demonstrate this computational advantage using a community velocity model (Lee et al., 2014) configured with 234 sources and 339 receivers on the free surface, mimicking a real seismic dataset (BASIN, 2018). The RENO computes the Helmholtz solutions for all 234×339 source-receiver pairs in a single query, while the baseline model requires increasing the batch size to parallelize across sources. Using an NVIDIA RTX A6000 GPU with a memory capacity of 46 GB, the RENO can complete the computation in a single batch, whereas the baseline model encounters an out-of-memory issue and must iterate over multiple batches. At a comparable memory footprint, the RENO exhibits a 30-fold speedup over the baseline model during inference.

Neural operators can be used with automatic differentiation for full waveform inversion (Yang et al., 2023; Zou et al., 2025). We conduct inversion experiments using the above configurations. The acceleration in forward modeling translates to a similar acceleration in inversion, provided comparable computing resources. Both models are timed over 40 epochs. Table 1 summarizes the runtime and GPU memory usage. Inversion consumes less memory than forward modeling due to a smaller batch size. Note that the comparison here is made between a RENO and a standard neural operator. The latter has been shown to be about two orders of magnitude faster than conventional numerical solvers like the spectral element method (Zou et al., 2024).

5 Discussion and Conclusions

In physics-informed machine learning, there are two primary directions: hard constraints and soft constraints. Hard constraints involve designing a model architecture whose output strictly obeys physical laws, regardless of training. Conversely, soft constraints typically involve a regularization term to be minimized during training, with a classic example being PINNs (Raissi et al., 2019). These methods differ in several key aspects. For example, models with hard constraints are often more efficient to train, because computing soft-constraint regularization terms may require extra model calls or numerical calculation. Furthermore, while hard constraints ensure exact physical consistency, soft constraints only achieve an approximation. In addition, soft constraints require more tuning effort due to the hyperparameter optimization needed for the regularization coefficient. On the other hand, they offer the flexibility to balance different terms when they are slightly contradictory. Table 2 summarizes these differences.

Soft constraints have dominated current research in seismology (Geng et al., 2025; Wang et al., 2026), owing to their ease of implementation. Making architectural changes needs significantly more effort. In this study, we propose RENO, a neural operator architecture that leverages a transformer backbone to enforce reciprocity as a hard constraint. The model obeys the imposed physical law by

Table 2: Comparison of physics-informed methods in machine learning: hard and soft constraints.

Constraint Type	Method	Training Efficiency	Physical Consistency	Tuning Effort	Flexibility
Hard	Embedded in Architecture	High	Exact	Low	Low
Soft	Regularization	Low	Approximate	High	High

design, without the need for specialized training. Training is instead used to learn other aspects of wave propagation physics. The RENO inherits the full capabilities of standard neural operators, while offering superior physical consistency and an order-of-magnitude computational speedup in multi-source scenarios. To start, the current architecture is designed for the reciprocity relation for particle velocity fields under single forces in the same direction, which is directly transferable to pressure fields under dilatational sources and travel-time fields governed by the eikonal equation. The framework supports various scientific applications, including ambient noise tomography, marine seismic surveys, and travel-time tomography. Future studies will address more complex reciprocity relations.

Data and Resources

We have open-sourced our code at <https://github.com/caifeng-zou/RENO>.

Acknowledgements

This material is based upon work supported by the U.S. Department of Energy, Office of Science, Office of Advanced Scientific Computing Research, Science Foundations for Energy Earthshot under Award Number DE-SC0024705. This research is also partially supported by NSF-2438773.

References

Alkhalifah, T., Song, C., bin Waheed, U., & Hao, Q., 2021. Wavefield solutions from machine learned functions constrained by the Helmholtz equation, *Artificial Intelligence in Geosciences*, **2**, 11–19.

Alkin, B., Fürst, A., Schmid, S., Gruber, L., Holzleitner, M., & Brandstetter, J., 2024. Universal physics transformers: A framework for efficiently scaling neural operators, *Advances in Neural Information Processing Systems*, **37**, 25152–25194.

Arntsen, B. & Carcione, J. M., 2000. A new insight into the reciprocity principle, *Geophysics*, **65**(5), 1604–1612.

Azizzadenesheli, K., Kovachki, N., Li, Z., Liu-Schiaffini, M., Kossaifi, J., & Anandkumar, A., 2024. Neural operators for accelerating scientific simulations and design, *Nature Reviews Physics*, **6**(5), 320–328.

BASIN, 2018. San Gabriel and San Bernardino Basin Arrays, Dataset.

Brocher, T. M., 2005. Empirical relations between elastic wavespeeds and density in the Earth's crust, *Bulletin of the Seismological Society of America*, **95**(6), 2081–2092.

Eisner, L. & Clayton, R. W., 2001. A reciprocity method for multiple-source simulations, *Bulletin of the Seismological Society of America*, **91**(3), 553–560.

Geng, H., Song, C., bin Waheed, U., & Liu, C., 2025. Seismic first-arrival traveltimesimulation based on reciprocity-constrained PINN, *Journal of Applied Geophysics*, p. 105967.

Graves, R. W. & Clayton, R. W., 1992. Modeling path effects in three-dimensional basin structures, *Bulletin of the Seismological Society of America*, **82**(1), 81–103.

Huang, X. & Alkhalifah, T., 2022a. PINNup: Robust neural network wavefield solutions using frequency upscaling and neuron splitting, *Journal of Geophysical Research: Solid Earth*, **127**(6), e2021JB023703.

Huang, X. & Alkhalifah, T., 2022b. Single reference frequency loss for multifrequency wavefield representation using physics-informed neural networks, *IEEE Geoscience and Remote Sensing Letters*, **19**, 1–5.

Huang, X. & Alkhalifah, T., 2025. Learned frequency-domain scattered wavefield solutions using neural operators, *Geophysical Journal International*, **241**(3), 1467–1478.

Knopoff, L. & Gangi, A. F., 1959. SEISMIC RECIPROCITY*, *Geophysics*, **24**(4), 681–691.

Kong, Q., Zou, C., Choi, Y., Matzel, E. M., Azizzadenesheli, K., Ross, Z. E., Rodgers, A. J., & Clayton, R. W., 2025. Reducing Frequency Bias of Fourier Neural Operators in 3D Seismic Wavefield Simulations Through Multistage Training, *Seismological Research Letters*, **97**(1), 272–282.

Lee, E.-J., Chen, P., Jordan, T. H., Maechling, P. B., Denolle, M. A., & Beroza, G. C., 2014. Full-3-D tomography for crustal structure in southern California based on the scattering-integral and the adjoint-wavefield methods, *Journal of Geophysical Research: Solid Earth*, **119**(8), 6421–6451.

Lehmann, F., Gatti, F., Bertin, M., & Clouteau, D., 2024. 3D elastic wave propagation with a factorized Fourier neural operator (F-FNO), *Computer Methods in Applied Mechanics and Engineering*, **420**, 116718.

Lehmann, F., Gatti, F., & Clouteau, D., 2025. Multiple-input fourier neural operator (mifno) for source-dependent 3d elastodynamics, *Journal of Computational Physics*, p. 113813.

Li, Z., Kovachki, N., Azizzadenesheli, K., Liu, B., Bhattacharya, K., Stuart, A., & Anandkumar, A., 2020a. Fourier neural operator for parametric partial differential equations, *arXiv preprint arXiv:2010.08895*.

Li, Z., Kovachki, N., Azizzadenesheli, K., Liu, B., Bhattacharya, K., Stuart, A., & Anandkumar, A., 2020b. Neural operator: Graph kernel network for partial differential equations, *arXiv preprint arXiv:2003.03485*.

Li, Z., Kovachki, N., Choy, C., Li, B., Kossaifi, J., Otta, S., Nabian, M. A., Stadler, M., Hundt, C., Azizzadenesheli, K., et al., 2023. Geometry-informed neural operator for large-scale 3d pdes, *Advances in Neural Information Processing Systems*, **36**, 35836–35854.

Li, Z., Zheng, H., Kovachki, N., Jin, D., Chen, H., Liu, B., Azizzadenesheli, K., & Anandkumar, A., 2024. Physics-informed neural operator for learning partial differential equations, *ACM/JMS Journal of Data Science*, **1**(3), 1–27.

Petrov, P. V. & Newman, G. A., 2019. Estimation of seismic source parameters in 3D elastic media using the reciprocity theorem, *Geophysics*, **84**(6), R963–R976.

Raiissi, M., Perdikaris, P., & Karniadakis, G. E., 2019. Physics-informed neural networks: A deep learning framework for solving forward and inverse problems involving nonlinear partial differential equations, *Journal of Computational physics*, **378**, 686–707.

Rasht-Behesht, M., Huber, C., Shukla, K., & Karniadakis, G. E., 2022. Physics-informed neural networks (PINNs) for wave propagation and full waveform inversions, *Journal of Geophysical Research: Solid Earth*, **127**(5), e2021JB023120.

Ren, P., Rao, C., Chen, S., Wang, J.-X., Sun, H., & Liu, Y., 2024. SeismicNet: Physics-informed neural networks for seismic wave modeling in semi-infinite domain, *Computer Physics Communications*, **295**, 109010.

Richardson, A., 2025. Deepwave.

Shi, Y., Ross, Z. E., Asimaki, D., & Azizzadenesheli, K., 2025. Mesh-Informed Neural Operator: A Transformer Generative Approach, *arXiv preprint arXiv:2506.16656*.

Song, C., Alkhalifah, T., & Waheed, U. B., 2021. Solving the frequency-domain acoustic VTI wave equation using physics-informed neural networks, *Geophysical Journal International*, **225**(2), 846–859.

Song, C., Alkhalifah, T., & Waheed, U. B., 2022. A versatile framework to solve the Helmholtz equation using physics-informed neural networks, *Geophysical Journal International*, **228**(3), 1750–1762.

Vaswani, A., Shazeer, N., Parmar, N., Uszkoreit, J., Jones, L., Gomez, A. N., Kaiser, L., & Polosukhin, I., 2017. Attention is all you need, *Advances in neural information processing systems*, **30**.

Wang, Y., Geng, H., Song, C., & Liu, C., 2026. Reciprocity-aware PINN-based seismic traveltime tomography and uncertainty quantification for models with irregular topography, *Geophysical Journal International*, **244**(3), ggag015.

Wu, H., Luo, H., Wang, H., Wang, J., & Long, M., 2024. Transolver: A fast transformer solver for pdes on general geometries, *arXiv preprint arXiv:2402.02366*.

Yang, Y., Gao, A. F., Castellanos, J. C., Ross, Z. E., Azizzadenesheli, K., & Clayton, R. W., 2021. Seismic wave propagation and inversion with neural operators, *The Seismic Record*, **1**(3), 126–134.

Yang, Y., Gao, A. F., Azizzadenesheli, K., Clayton, R. W., & Ross, Z. E., 2023. Rapid seismic waveform modeling and inversion with neural operators, *IEEE Transactions on Geoscience and Remote Sensing*, **61**, 1–12.

Zhao, L., Chen, P., & Jordan, T. H., 2006. Strain Green’s tensors, reciprocity, and their applications to seismic source and structure studies, *Bulletin of the Seismological Society of America*, **96**(5), 1753–1763.

Zou, C., Azizzadenesheli, K., Ross, Z. E., & Clayton, R. W., 2024. Deep neural Helmholtz operators for 3-D elastic wave propagation and inversion, *Geophysical Journal International*, **239**(3), 1469–1484.

Zou, C., Ross, Z. E., Clayton, R. W., Lin, F.-C., & Azizzadenesheli, K., 2025. Ambient noise full waveform inversion with neural operators, *Journal of Geophysical Research: Solid Earth*, **130**(11), e2025JB031624.